



High-frequency magnetotransport in a viscous electron fluid under a Stern-Gerlach forceYa Zhang ¹, Feng Zhai,^{2,*} and Wei Jiang ^{3,†}¹*Department of Physics, Wuhan University of Technology, Wuhan 430070, China*²*Department of Physics, Zhejiang Normal University, Zhejiang 321004, China*³*School of Physics, Huazhong University of Science and Technology, Wuhan 430074, China*

(Received 11 July 2021; revised 1 October 2021; accepted 7 October 2021; published 22 October 2021)

We apply a hydrodynamic theory to study transverse magnetosonic resonances in a viscous two-dimensional electron fluid under an in-plane Stern-Gerlach force (SGF), a perpendicular magnetic field with cyclotron frequency ω_c , and an alternating electric field with frequency ω . The SGF leads to a splitting in the dispersion curve of the transverse magnetosound wave and hinders the long-wavelength plasmonic excitation. The effective diagonal viscosity coefficient can be enhanced by about one order of magnitude due to the SGF. The variation of absorption power Y with ω_c exhibits a viscoelastic (VE) resonance at $\omega_c = \omega/2$ and transverse magnetosound resonances. The SGF can raise the heights of all resonant peaks and leave the peak positions almost completely unchanged. The most substantial magnetosonic resonant peak, much weaker than the VE peak in the absence of SGF, can be tuned by the SGF to be well above the VE peak. Our results indicate that the SGF can be used to tune the VE resonance and transverse magnetosound resonances, which is relevant to the manipulation of photoresistance and photovoltaic effects in viscous electron fluids.

DOI: [10.1103/PhysRevB.104.165139](https://doi.org/10.1103/PhysRevB.104.165139)**I. INTRODUCTION**

In clean materials, electrons can form viscous flow in a hydrodynamic regime at low temperatures when momentum-conserving interparticle collisions are much more dominant than any other collisions that cannot conserve momentum [1]. A hydrodynamic regime can be formed when the mean free path of electron-electron scattering (l_{ee}) is the shortest one compared to those of electron-phonon and electron-disorder collisions (l), i.e., $l_{ee} \ll l$, where the motion of viscous electrons becomes collective and can be described by a hydrodynamic model [2–5]. Bright evidence of the hydrodynamic regime of electron transport has been reported in novel nanostructures [6–10], such as high-mobility quantum wells, monovalence layered metal PdCoO₂, and three-dimensional Weyl semimetal WP₂. The experimental reports of hydrodynamic transport have been accompanied by intense interest of theoretical studies [2–5].

Giant negative magnetoresistance in viscous electron fluids has attracted much research interest, where the resistance decreased by several orders of magnitude in moderate magnetic fields relative to the zero magnetic field, showing numerous mysterious characteristics [6–10]. The giant negative magnetoresistance effect has been discussed in the frame of hydrodynamic models considering the dependence of the electron viscosity coefficients on magnetic field [2] and on a Stern-Gerlach force (SGF) [5]. A viscous electron flow in the hydrodynamic regime was studied, and the sample resistance was proportional to the diagonal viscosity coefficient

provided that the electron-electron scattering dominates [2], yielding the giant negative magnetoresistance. It was shown that the presence of SGF in a spin-dependent viscous flow could enhance the giant negative magnetoresistance effect, manifesting in the fact that the effective diagonal viscosity of the fluid was enhanced by about three orders of magnitude at zero magnetic field [5].

High-frequency transport of a viscous two-dimensional (2D) electron fluid in zero magnetic field flowing along an extended sample has been theoretically studied in Refs. [11,12]. Transverse zero sound was studied in a 2D strongly interacting Fermi liquid [13,14]. Alekseev *et al.* [3,4,15] developed a hydrodynamic theory for high-frequency magnetotransport in a highly viscous fluid in GaAs/GaAlAs heterostructure, where transverse magnetosonic waves and conventional magnetoplasmons were reported. The electron shear viscosity coefficient has shown the so-called viscoelastic (VE) resonance [3] when the alternating current (AC) frequency ω and the cyclotron frequency ω_c satisfy $\omega = 2\omega_c$. It was pointed out that [4] the transverse zero magnetosound can be excited in a highly nonideal Fermi gas, which was guaranteed by the fact that the shear viscosity coefficient was significantly enhanced compared to that in an ideal Fermi system. The hydrodynamic Navier-stokes equation can be derived from the kinetic equation in a nonideal Fermi gas with strongly interacting quasiparticles, which confirms the feasibility of the hydrodynamic approach of transverse zero magnetosound in a highly viscous 2D nonideal fluid [4].

However, the transverse zero magnetosound has not been studied in a spin-dependent viscous electron flow in the hydrodynamic regime. In this work, we predict excitations of transverse zero magnetosounds in a spin-dependent viscous two-dimensional electron gas (2DEG) modulated by an

*fzhai@zjnu.cn

†weiji Jiang@hust.edu.cn

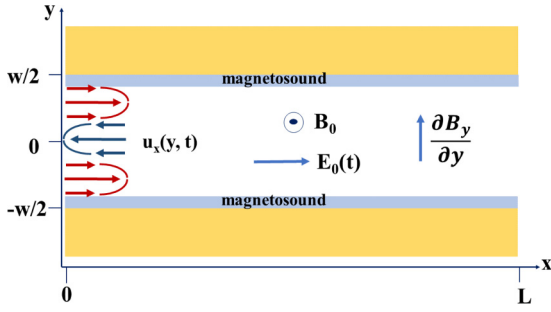


FIG. 1. Schematic illustration of a 2DEG sample with length L , width W , and rough edges. The configurations of external fields include a constant perpendicular magnetic field B_0 , an AC electric field along the x axis, and a constant magnetic field gradient ∇B_y along the y axis. The hydrodynamic velocity $u_x(y, t)$ shows a standing-wave-like distribution.

in-plane SGF, a perpendicular magnetic field, and an AC electric field. A two-component hydrodynamic approach taking into account the frequency and spin dependence of viscosity is used to study the effect of in-plane SGF on the shear viscosity coefficients. We show that the viscosity coefficients are enhanced by about one order of magnitude due to the SGF, which is useful for realizing the transverse magnetosonic wave propagating in a viscous Fermi fluid. This provides a possible route to excite transverse zero magnetosounds even in an ideal Fermi gas, manifesting that the transverse magnetosonic resonances can be enhanced significantly by the SGF to be much higher than the VE resonance.

II. MODEL AND FORMALISM

We consider a 2DEG in the (x, y) plane with width W along the y direction and length L along the x direction, which is subject to a constant magnetic field B_0 along the z direction, an AC electric field $E_0(t)$ along the x direction, and a constant magnetic field gradient ∇B_y along the y direction. The spin quantization direction is taken to be the y axis [5]. The geometry and fields under consideration are presented in Fig. 1.

High-frequency dynamics of a spin-dependent viscous electron fluid can be described by a two-component Fermi liquid model with the spin-dependent particle density $n_s(\mathbf{r}, t) = n_0 + \delta n_s(\mathbf{r}, t)$ and the fluid velocity $\mathbf{u}_s(\mathbf{r}, t)$. Here $\mathbf{r} = (x, y)$ is a position in the 2DEG, $s = \pm 1$ represents the spin-up and spin-down subsystem, and n_0 is the equilibrium density for both spin-up and spin-down electrons under zero field. The total hydrodynamic density and velocity are given by $n(\mathbf{r}, t) = n_+(\mathbf{r}, t) + n_-(\mathbf{r}, t)$ and $\mathbf{u}(\mathbf{r}, t) = \mathbf{u}_+(\mathbf{r}, t) + \mathbf{u}_-(\mathbf{r}, t)$.

The linearized continuity and Navier-Stokes equations can be derived by assuming a time dependence $e^{-i\omega t}$ for the total and spin-dependent hydrodynamic velocities,

$$\begin{aligned} -i\omega\delta n_s + n_0\nabla\cdot\mathbf{u}_s &= 0, \\ -i\omega\mathbf{u}_s &= \omega_c\mathbf{u}_s \times \mathbf{e}_z + \frac{e}{2m}\mathbf{E}(\mathbf{r}, \omega) - \frac{\mathbf{u}_s}{\tau} + \frac{\eta_{xx1}(\omega)}{2}\nabla^2\mathbf{u} \\ &+ \frac{\eta_{yx1}(\omega)}{2}\nabla^2\mathbf{u} \times \mathbf{e}_z + s\frac{g^*\mu_B}{4m}\nabla B_y, \end{aligned} \quad (1)$$

where $\nabla = \frac{\partial}{\partial x}\mathbf{e}_x + \frac{\partial}{\partial y}\mathbf{e}_y$, e is the fundamental charge, m is the effective electron mass, $\omega_c = eB_0/mc$ with c the light speed, $\mathbf{E}(\mathbf{r}, \omega)$ is the complex amplitudes of the harmonics of the electric field $\mathbf{E}(\mathbf{r}, t)$, and $1/\tau$ is the rate of momentum relaxation in bulk due to the electron scattering on disorder and/or phonons [2]. The magnetic field gradient yields the spin-dependent SGF $s\frac{g^*\mu_B}{4}\frac{\partial B_y}{\partial y}$, where g^* is the effective g factor, and μ_B is the Bohr magneton. The effective shear viscosity coefficients $\eta_{xx1}(\omega)$ and $\eta_{yx1}(\omega)$ depend on the SGF, magnetic field (B_0), and AC frequency (ω),

$$\begin{aligned} \eta_{xx1}(\omega) &= \frac{1 - i\omega\tau_2}{1 + (-\omega^2 + 4\omega_c^2)\tau_2^2 - 2i\omega\tau_2}\eta \\ &+ \left[\frac{(1 - i\omega\tau_2)}{1 + (-\omega^2 + 4\omega_c^2)\tau_2^2 - 2i\omega\tau_2} \frac{\tau_2 g^* \mu_B}{2m} \frac{\partial B_y}{\partial y} \right]^2 \frac{\tau}{4}, \end{aligned} \quad (2)$$

$$\begin{aligned} \eta_{yx1}(\omega) &= \frac{2\omega_c\tau_2}{1 + (-\omega^2 + 4\omega_c^2)\tau_2^2 - 2i\omega\tau_2}\eta \\ &+ \frac{(1 - i\omega\tau_2)(2\omega_c\tau_2)}{[1 + (-\omega^2 + 4\omega_c^2)\tau_2^2 - 2i\omega\tau_2]^2} \\ &\times \left(\frac{\tau_2 g^* \mu_B}{2m} \frac{\partial B_y}{\partial y} \right)^2 \frac{\tau}{4}. \end{aligned} \quad (3)$$

The expressions of η_{xx1} and η_{yx1} are derived in Appendix A. Here η is the viscosity coefficient without B_0 and SGF, and τ_2 is the relaxation time of the second angular momentum of the distribution function with respect to velocity, which are the same as in Refs. [3,4]. In Ref. [15], Eq. (1) was consistently derived from the kinetic equation for strongly interacting Fermi-liquid quasiparticles, where the value of η becomes $\eta = v_{F\eta}^2\tau_2/4$. In this case the parameter $v_{F\eta} = 2\sqrt{\eta/\tau_2}$ is quite larger than its counterpart v_F , where $v_F = \hbar\sqrt{4\pi n_0}/m$ (\hbar is the Plank constant) is the Fermi velocity. Otherwise, $\eta = v_F^2\tau_2/4$ in a nearly ideal Fermi gas [2,3,5]. For a high-frequency flow with characteristic frequencies $\omega, \omega_c \gg 1/\tau_2$, the effective viscosity coefficients lead to the VE resonance at $\omega = 2\omega_c$. Note that the hydrodynamic pressure term $-\nabla P/m$ is neglected, and the electron fluid is considered as incompressible ($\nabla\cdot\mathbf{u} = 0$) as in Refs. [2,3,5].

We derive the linearized continuity and Navier-Stokes equations of total density perturbation and velocity by adding and subtracting over the spin index in Eq. (1),

$$-i\omega\delta n + n_0\nabla\cdot\mathbf{u} = 0, \quad (4)$$

$$\begin{aligned} -i\omega\mathbf{u} &= \frac{e}{m}\mathbf{E}(\mathbf{r}, \omega) + \omega_c\mathbf{u} \times \mathbf{e}_z - \frac{\mathbf{u}}{\tau} \\ &+ \eta_{xx1}(\omega)\nabla^2\mathbf{u} + \eta_{yx1}(\omega)[\nabla^2\mathbf{u} \times \mathbf{e}_z], \end{aligned} \quad (5)$$

where $\delta n = \delta n(\mathbf{r}, \omega)$ and $\mathbf{u} = \mathbf{u}(\mathbf{r}, \omega)$ are the complex amplitudes of the perturbed particle density $\delta n(\mathbf{r}, t) = n(\mathbf{r}, t) - n_0$ and the hydrodynamic velocity $\mathbf{u}(\mathbf{r}, t)$.

The hydrodynamic model [Eqs. (4) and (5)] has been validated and applied when the interparticle scattering length $\propto \tau_2 v_F$ is the shortest one [2–5,17]. The hydrodynamic method can be applicable under the condition that a fluid flow is driven by a high-frequency external electric field with frequency ω

fulfilling $\omega \gg 1/\tau_2$, where the quasiequilibrium distribution of electrons in the moving frame does not have enough time to be formed. This condition has been indeed realized for transverse zero sound in a strongly nonideal electron liquid [4,15,17].

It is instructive to seek the wavelike solutions of Eqs. (4) and (5) without the external electric field ($\mathbf{E}_0 = 0$), that is, the plasmonic excitation. For a plane wave propagating along the x axis with a complex frequency ω and real wave vector q , the velocity and Hall electric field can be written as

$$\begin{aligned} u_x(y, t) &= u_{x0} \exp(-i\omega t + iqy), \\ E_y(y, t) &= E_{y0} \exp(-i\omega t + iqy). \end{aligned}$$

Here we adopt the condition $u_y = u_{sy} \equiv 0$. The Navier-Stokes Eq. (5) yields a closed set of equations for the amplitudes u_{x0} and E_{y0} ,

$$\begin{aligned} i\omega u_{x0} - \frac{1}{\tau} u_{x0} - \eta_{xx1} u_{x0} q^2 &= 0, \\ \frac{e}{m} E_{y0} - \omega_c u_{x0} + \eta_{yx1} u_{x0} q^2 &= 0. \end{aligned} \quad (6)$$

The solution corresponds to the waves of transverse zero sound, where $\mathbf{u} \perp \mathbf{q}$ describes the transverse character of the magnetosonic waves, due to $\nabla \cdot \mathbf{u} = 0$ and $\delta n = 0$ [see Eq. (4)]. These kinds of waves are different from conventional magnetoplasmons. The transverse character of the magnetosonic waves[4] are induced by perturbations of the shear stress tensor and are analogous to transverse sound in amorphous solids [18].

In Eq. (6) the complex frequency ω depends on the real wave vector q , $\omega = \omega_q - i\Upsilon_q$. The dispersion relation ω_q and damping coefficient Υ_q of the transverse zero magnetosound are determined from

$$i(\omega_q - i\Upsilon_q) - 1/\tau - \eta_{xx1} q^2 = 0. \quad (7)$$

This equation yields

$$\omega_q = \text{Im}(\eta_{xx1}) q^2, \quad (8)$$

$$\Upsilon_q = \left[\frac{1}{\tau} + \text{Re}(\eta_{xx1}) q^2 \right] / [1 - q^2 \text{Im}(\eta'_{xx1})], \quad (9)$$

where $\eta_{xx1}(\omega)$ and its derivative $\eta'_{xx1}(\omega)$ are calculated at $\omega = \omega_q$ for small Υ_q . Thus the dispersion of the transverse magnetosonic wave is determined by the frequency-dependent diagonal viscosity coefficient η_{xx1} . At high frequencies ($\omega_c, \omega_q \gg 1/\tau_2 > 1/\tau$) and far from the VE resonance ($|\omega_q - 2\omega_c| \gg 1/\tau_2$), based on Eqs. (2), (8), and (9) one can approximate the transcendental equation of dispersion relation and damping coefficient as

$$(\omega_q^2 - 4\omega_c^2)^2 - \frac{\eta q^2}{\tau_2} (\omega_q^2 - 4\omega_c^2) + \alpha \frac{v_F^2 \eta q^2}{2\tau_2^2} = 0, \quad (10)$$

$$\Upsilon_q = \frac{(4\omega_c^2 - \omega_q^2)^2 - \alpha \omega_q^2 (4\omega_c^2 - \omega_q^2)}{2\omega_q^2 \tau_2 (4\omega_c^2 - \omega_q^2 + 4\alpha/\tau_2^2)}, \quad (11)$$

where

$$\alpha = \frac{F^2 \tau \tau_2}{v_F^2 \eta}, \quad F = \frac{g^* \mu_B \partial B_y}{2m \partial y}. \quad (12)$$

The details for the derivation of Eqs. (10) and (11) are given in Appendix B.

Then we study the linear response of the electron fluid in a finite sample under a linearly polarized homogeneous AC electric field $\mathbf{E}_0(t) = E_0 \mathbf{e}_x e^{-i\omega t} + \text{c. c.}$. The velocity and the Hall electric field take the form $u_x(y, t) = u_x(y) e^{-i\omega t} + \text{c. c.}$ and $E_y(y, t) = E_y(y) e^{-i\omega t} + \text{c. c.}$ with a real frequency ω . The Navier-Stokes equation [Eq. (5)] leads to

$$\begin{pmatrix} i\omega + \eta_{xx1} \frac{d^2}{dy^2} - \frac{1}{\tau} & 0 \\ -\omega_c - \eta_{yx1} \frac{d^2}{dy^2} & 1 \end{pmatrix} \begin{pmatrix} u_x(y) \\ \frac{e}{m} E_y(y) \end{pmatrix} = -\frac{eE_0}{m} \begin{pmatrix} 1 \\ 0 \end{pmatrix}. \quad (13)$$

The solution of these differential equations can be expressed in terms of the characteristic wave vector

$$\lambda = \sqrt{-\frac{i\omega}{\eta_{xx1}} + \frac{1}{\tau \eta_{xx1}}}. \quad (14)$$

The velocity $u_x(y)$ is calculated under the boundary condition for the rough sample edges $\mathbf{u}|_{y=\pm W/2} = 0$, which is given by

$$u_x(y) = \frac{1}{-i\omega + 1/\tau} \frac{eE_0}{m} \left(1 - \frac{\cosh(\lambda y)}{\cosh(\lambda W/2)} \right). \quad (15)$$

The first and second terms in this velocity distribution are the bulk (Ohmic) and the viscosity-dependent term in the linear response, respectively. Based on Eq. (15), the total electric current

$$I_x = en \int_{-W/2}^{W/2} dy u_x(y)$$

can be expressed as

$$I_x = \frac{1}{-i\omega + 1/\tau} \frac{e^2 n_0 E_0 W}{m} \left(1 - \frac{\tanh(\lambda W/2)}{W \lambda/2} \right). \quad (16)$$

The linear response of $\mathbf{u}(y, t)$ also describes energy absorption and AC impedance from the AC external electric field $\mathbf{E}_0(t)$. The absorption power is written as

$$Y = 2E_0 \text{Re} I_x, \quad (17)$$

which can be calculated from Eqs. (14) and (16). The AC impedance is $Z = E_0/I_x$.

III. RESULTS AND DISCUSSION

It was reported that a highly viscous fluid could be formed in high-mobility GaAs 2DEG [2]. In InSb 2DEG, the viscosity coefficients are even higher than those in GaAs 2DEG [5]. Our results are obtained for an InSb [5,19,20] 2DEG. The parameters are chosen as $n_0 = 0.5 \times 10^{10} \text{ cm}^{-2}$, electron mobility $\mu \approx 10^5 \text{ cm}^2/\text{V s}$, $g^* = 40$, $m = 0.018m_e$, temperature $T = 1 \text{ K}$, and $\tau_2/\tau = 10^{-7}$. These parameters determine the possible range of α as 0.1–1000 for [4,5] $\frac{\partial B_y}{\partial y} = 8 \times 10^6$ to $8 \times 10^8 \text{ G cm}^{-1}$. In order to show how transverse zero magnetosonic waves are excited, it is necessary to employ a spatially nonuniform flow which is driven by a uniform AC electric field $\mathbf{E}_0(t) = E_0 e^{-i\omega t} \mathbf{e}_x$ and under no-slip boundary along the y direction.

Plasmon dispersion. In Fig. 2, the dispersion relation of the transverse magnetosound is shown in the absence ($\alpha = 0$) or presence ($\alpha = 10$) of SGF. The frequency ω and wave vector

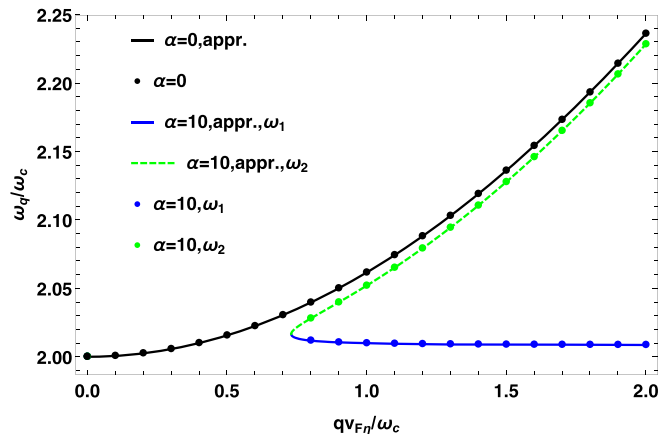


FIG. 2. Dispersion relation of the transverse magnetosound wave ω_q at fixed $\omega_c\tau_2 = 24.5$. The frequency ω is in units of ω_c and the wave number q is in units of $\omega_c/v_F\eta$. The solid and dashed lines show the approximate dispersion given by Eq. (10), while the circles are obtained from Eq. (8). The dispersion in the absence of SGF ($\alpha = 0$) is the same as in Ref. [4]. Two eigenvalues (ω_1 and ω_2) exist in the presence of SGF ($\alpha = 10$).

q are respectively in units of ω_c and $\omega_c/v_F\eta$. We take $\omega_c\tau_2 = 24.5$.

The dispersion in the absence of SGF (black circles in Fig. 2) is the same as in Ref. [4], which partly validates our calculations. The approximation results from Eq. (10) (black solid line in Fig. 2) coincide with those obtained by directly solving Eq. (8) numerically. This demonstrates the reliability of the analytical estimation of the diagonal viscosity coefficient η_{xx1} at high frequencies and far from the VE resonance. At $q = 0$ the plasmon frequency $\omega = 2\omega_c$ is explained by the own rotation of the shear stress tensor of the viscous fluid in magnetic field [4].

As shown in Fig. 2, in the presence of SGF the approximate dispersion obtained from Eq. (10) still agrees well with the numerically exact solution. From Eq. (10) one yields the analytical dispersion expression for $q \geq q_{th} = \sqrt{32\alpha}/(\omega_c\tau_2)$,

$$\omega_{1,2} = \frac{\omega_c}{2\sqrt{2}} \sqrt{32 + q^2 \mp \frac{q}{\omega_c\tau_2} \sqrt{-32\alpha + q^2\omega_c^2\tau_2^2}}. \quad (18)$$

Note that the transverse magnetosound wave is absent at $q < q_{th}$ in the presence of SGF, as shown in Fig. 2. The SGF hinders plasmon excitation in the long-wavelength limit. This observation is consistent with the following relation required for realizing the transverse magnetosound wave [4]:

$$(2k + 1) \frac{\pi}{q(\omega_q, \omega_c)} = W. \quad (19)$$

Here k is integer and $q(\omega_q, \omega_c) \geq q_{th}$ is the wave number of the magnetosound wave obtained from Eq. (10). Equation (19) claims that the sample width W should be an odd number of the half wavelength $\Lambda_h = \pi/q(\omega_q, \omega_c)$ of the magnetosound standing wave. Due to the non-slip condition $u|_{y=\pm W/2} = 0$, the ratio W/Λ_h should be integer. The magnetosound standing wave has a finite contribution to the current I_x only when the integer W/Λ_h is odd.

Two eigenvalues (ω_1 and ω_2) exist in the presence of SGF ($\alpha = 10$ in Fig. 2) at $q \geq q_{th}$. This corresponds to two

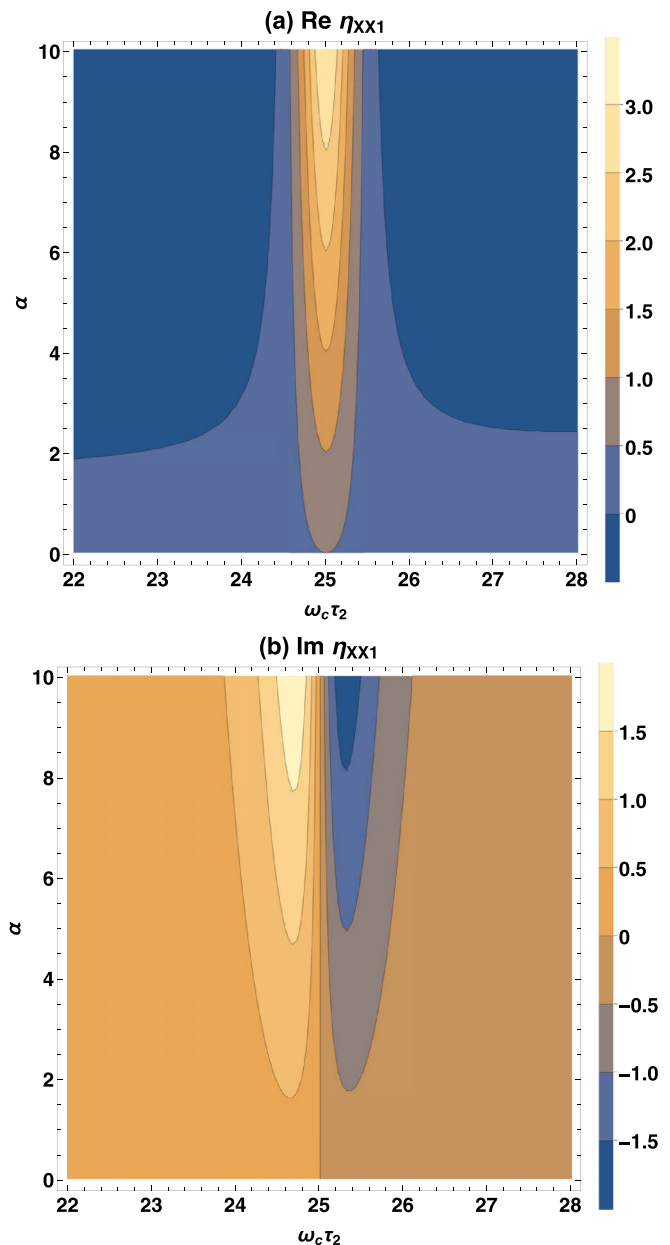


FIG. 3. The dissipative parts of the viscosity coefficients in units of $\eta = v_F^2\tau_2/4$, (a) $\text{Re } \eta_{xx1}$ and (b) $\text{Im } \eta_{xx1}$, plotted as functions of $\omega_c\tau_2$ and α at $\omega\tau_2 = 50$.

branches of the transverse magnetosound wave. The branch ω_2 with a remarkable dispersion lies below the dispersion curve for $\alpha = 0$. The two curves (ω_2 and $\omega_q|_{\alpha=0}$) tend to coincide for large wave vectors. The branch ω_1 decreases from its maximum $\omega_{1th} = 2\sqrt{1 + \alpha/\omega_c^2\tau_2^2}$ to $2\omega_c$ as the wave vector increases from q_{th} . This new branch of transverse magnetosound wave is almost nondispersive.

Tuning the AC viscosity by SGF. The tunability of the dispersion relation by the SGF results from the effective diagonal viscosity coefficient η_{xx1} [see Eq. (8)]. Figure 3 shows the effective diagonal viscosity coefficient η_{xx1} (normalized by $\eta = v_F^2\tau_2/4$) as functions of $\omega_c\tau_2$ and α for a fixed $\omega\tau_2 = 50$.

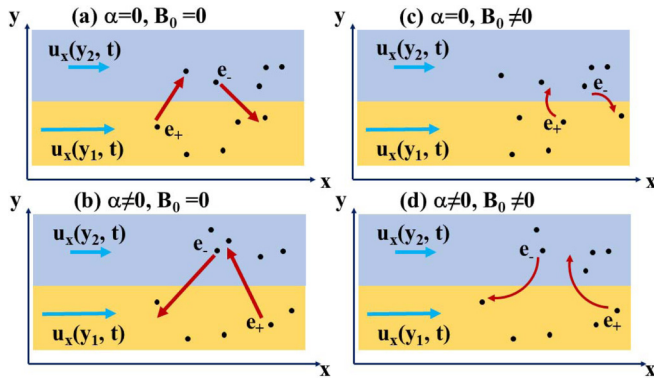


FIG. 4. Schematic illustration of the physical origin for the modification of effective viscosity coefficients ($\text{Re } \eta_{xx1}$ and $\text{Im } \eta_{xx1}$). The electron fluids in two adjacent layers move with different velocities $u_x(y_1, t)$ and $u_x(y_2, t)$. The viscosity is determined by the interlayer penetration length [2] of electrons. Here e_+ and e_- represents spin-up and spin-down electrons. (a) $\alpha = 0, B_0 = 0$; (b) $\alpha \neq 0, B_0 = 0$; (c) $\alpha = 0, B_0 \neq 0$; (d) $\alpha \neq 0, B_0 \neq 0$.

At $\alpha = 0$, Eq. (2) is reduced to that in Ref. [4]. The real part of η_{xx1} reaches its maximum 0.5 at the VE resonance point $\omega_c \tau_2 = \omega \tau_2 / 2$. At a finite α , $\text{Re } \eta_{xx1}$ is still peaked at $\omega_c \tau_2 = \omega \tau_2 / 2$ with full width at half maximum $\omega_c \tau_2$. Its maximum is $0.5(1 + \alpha/2)$, which increases with α [see Fig. 3(a)]. The maximum at $\alpha = 10$ is six times larger than that at $\alpha = 0$. This indicates that the SGF can enhance the nonlinear resonance and thus alter transport properties of high-frequency viscous flow. At the VE resonance, the imaginary part of η_{xx1} is almost unaffected by the SGF due to $\omega \tau_2 \gg 1$. For $\omega_c \tau_2$ near the VE resonance, the curve $\text{Im } \eta_{xx1}$ is almost antisymmetric. The maximum of $\text{Im } \eta_{xx1}$ increases from 0.22 to 1.8 as α varies from 0 to 10. The peak width of $\text{Im } \eta_{xx1}$ is about $\omega_c \tau_2$ in all cases. These features could be understood from Eq. (2).

The SGF-induced modification of effective viscosity coefficient ($\text{Re } \eta_{xx1}$ and $\text{Im } \eta_{xx1}$) could be explained by means of Fig. 4. The viscosity arises from the exchange of electrons [2] between two adjacent layers of electron fluid moving with different velocities $u_x(y_1, t)$ and $u_x(y_2, t)$. For $\alpha = 0$ and $B_0 = 0$ [Fig. 4(a)], the interlayer penetration length of electrons is of the order $l_2 = v_{F\eta} \tau_2$. As the transverse SGF turns on [Fig. 4(b)], spin-up (-down) electrons from the lower (upper) layer can penetrate on a larger distance into another one. As a result, the viscosity friction determined by the penetration length can be enhanced by the SGF. Under a perpendicular magnetic field with cyclotron radius $R_c = v_{F\eta} / \omega_c < l_2$, the penetration length is limited by the cyclotron radius [Fig. 4(c)] and decreases with the magnetic field. Such a limitation could be relaxed when the SGF is applied [Fig. 4(d)]. Therefore, the viscosity reduced by the magnetic field can be enhanced by the SGF, as demonstrated theoretically in Ref. [5] in the case of direct current. In the presence of an AC electric field with frequency ω , such an enhancement can be further amplified around the VE resonance $\omega_c = \omega/2$.

Control of alternating current and absorption power by SGF. The SGF dependence of effective viscosity can be reflected in measurable quantities such as the alternating current (I_x), absorption power (Y), and AC impedance (Z). In Figs. 5

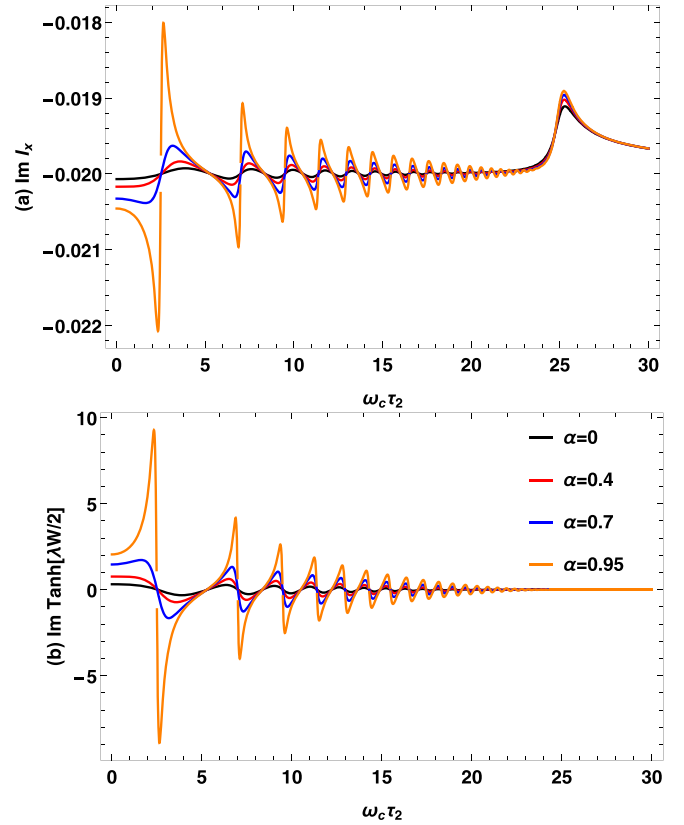


FIG. 5. (a) The imaginary part of the alternating current $\text{Im } I_x$ in units of $I_{x0} = e^2 n_0 W E_0 \tau_2 / m$ plotted as a function of $\omega_c \tau_2$. (b) Variation of $\text{Im } \tanh(\lambda W/2)$ as a function of $\omega_c \tau_2$. We set $\omega \tau_2 = 50$, $\tau_2 / \tau = 10^{-7}$, $W/l_2 = 1.8$, and $\alpha = 0, 0.4, 0.7, 0.95$. The VE resonance and the magnetosonic resonances are seen for all curves.

and 6 we plot the alternating current (I_x) and absorption power (Y) as a function of $\omega_c \tau_2$ under several values of α at fixed $\omega \tau_2 = 50$ and $\tau_2 / \tau = 10^{-7}$. The width of the sample is taken as $W = 1.8l_2$, where $l_2 = v_{F\eta} \tau_2$ is a characteristic length. For this medium width, the plasmonic contribution can be neglected.

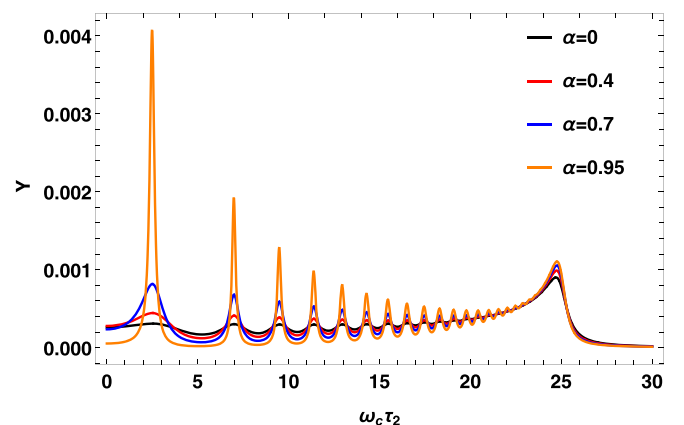


FIG. 6. The absorption power Y in units of Y_0 plotted as a function of $\omega_c \tau_2$. We set $\omega \tau_2 = 50$, $\tau_2 / \tau = 10^{-7}$, $W/l_2 = 1.8$, and $\alpha = 0, 0.4, 0.7, 0.95$.

In all curves, one can observe an asymmetric resonant peak at $\omega_c \tau_2 = \omega \tau_2 / 2$. As shown in Figs. 5 and 6, the amplitude of this VE resonance increases with α . Near the VE resonance ($|\omega - 2\omega_c| \lesssim 1/\tau_{ee}$), the wave vector λ defined in Eq. (14) can be approximated as

$$\lambda \approx \frac{2(4\omega_c^2 - \omega^2 - 2i\omega/\tau_2)}{\sqrt{(4\omega_c^2 - \omega^2 - 2i\omega/\tau_2)v_{F\eta}^2 - \omega F^2 \tau}}. \quad (20)$$

Near the right side of the VE resonance, $|\text{Re } \lambda|$ increases drastically while $|\text{Im } \lambda|$ is small. Accordingly, $u_x(y)$ decays quickly from edges to the bulk, leading to an edge VE flow. When ω_c moves down from $\omega/2$, $|\text{Im } \lambda|$ increases quickly while $|\text{Re } \lambda|$ is small. The corresponding $u_x(y)$ profile shows remarkable spatial oscillations (see Appendix C). For the high-frequency linear response near the VE resonance, the absorption power Y can be obtained from Eqs. (16) and (20) under the approximation $\tanh(W\lambda/2) \sim 1$,

$$Y(\omega_c) \approx \frac{Y_0}{2W/l_2} \text{Re} \left(\frac{\sqrt{i - (2\omega_c - \omega)\tau_2 + \alpha/2}}{i - (2\omega_c - \omega)\tau_2} \right), \quad (21)$$

$$Y_0 = e^2 n_0 W E_0^2 \tau_2 / m. \quad (22)$$

This equation results in an asymmetric VE resonant peak at $\omega_c = \omega/2$ with amplitude $\sqrt{(1 + \sqrt{1 + 0.25\alpha^2})/2} \frac{Y_0 l_2}{2W}$. Consequently, one can understand the enhancement of the VE peak by the SGF.

In Figs. 5 and 6, one can also observe a series of resonant peaks for $\omega_c < \omega/2$. Such resonances are named as ‘‘transverse magnetosound resonances’’ or ‘‘magnetosonic resonances’’ [4]. They arise from the formation of standing waves of transverse zero sound under the condition Eq. (19). The application of SGF can greatly enhance the magnetosonic resonances but almost unchanged the peak positions. As shown in Fig. 5(b), the oscillation amplitude of magnetosonic resonances is mainly controlled by the factor $\text{Im } \tanh(\lambda W/2)$.

Away from the VE resonance where $2\omega_c - \omega \gg 1/\tau_2$, one can approximate the wave vector λ in Eq. (14) as

$$\begin{aligned} \lambda &\approx \frac{2|4\omega_c^2 - \omega^2|}{\sqrt{(4\omega_c^2 - \omega^2)v_{F\eta}^2 - i\omega F^2 \tau}} \\ &\approx \frac{\sqrt{|\omega^2 - 4\omega_c^2|}}{v_{F\eta}} \left(2 + i \frac{\alpha\omega}{|\omega^2 - 4\omega_c^2|\tau_2} \right). \end{aligned} \quad (23)$$

After some algebra, one gets

$$\begin{aligned} -\text{Im } \tanh \frac{\lambda W}{2} &\approx \frac{\sin X}{\cos X + \cosh A}, \\ X &= \alpha \frac{\omega}{\sqrt{|\omega^2 - 4\omega_c^2|}} \frac{W}{l_2}, \\ A &= 2\tau_2 \sqrt{|\omega^2 - 4\omega_c^2|} \frac{W}{l_2}. \end{aligned} \quad (24)$$

The first maximum of this function increases quickly with α .

The values of absorption power at the first peak of magnetosonic resonances ($Y_{\text{FPMS}} \times 10^3$) and VE resonance

TABLE I. Absorption power at the first peak of magnetosonic resonances ($Y_{\text{FPMS}} \times 10^3$) and VE resonance ($Y_{\text{VE}} \times 10^3$) for different α .

	$\alpha = 0$	0.4	0.7	0.8	0.9	0.95
$Y_{\text{FPMS}} \times 10^3$	0.25	0.45	0.83	1.2	2.2	4.1
$Y_{\text{VE}} \times 10^3$	0.85	0.95	1.05	1.05	1.05	1.05

($Y_{\text{VE}} \times 10^3$) are shown for different α in Table I. The first maximum of absorption power at $\alpha = 0.95$ exceeds 16 times that at $\alpha = 0$ (see Fig. 6 and Table I). Such a SGF-induced resonance enhancement is more pronounced than that for the VE resonance. In the absence of SGF, the VE peak is much higher than all magnetosonic resonant peaks. Under the SGF with $\alpha = 0.95$, the amplitude of the first magnetosonic resonance is four times higher than that of the VE resonance, as shown in Table I.

The VE resonances and magnetosonic resonances are distinct in the SGF dependence because they are affected in different ways by the effective diagonal viscosity coefficient η_{xx1} . Such a distinction is partly reflected in Eqs. (21) and (24), which is also manifested in the profiles of hydrodynamic velocity (shown in Appendix C). Since the SGF is along the transverse direction, intuitively it has a stronger effect on the transverse character of the magnetosonic waves than that on the VE resonance. The transverse magnetosound waves are related to perturbations of shear stress of a charged Fermi liquid under a magnetic field. The perturbations can be enhanced greatly by the SGF. In comparison, the viscoelastic resonance is due to the intrinsic dynamics [15] of shear stress of charged fluids under a magnetic field. The presence of SGF could modify it only slightly.

Width dependence of SGF-induced resonance enhancement. The VE resonance and the transverse magnetosound resonances manifest themselves in different ways which depends on the normalized sample width W/l_2 . Figure 7 presents the absorption power Y as a function of $\omega_c \tau_2$ at $\omega \tau_2 = 50$ and $\tau_2/\tau = 10^{-7}$ in the presence ($\alpha = 0.9$) or absence ($\alpha = 0$) of the SGF. The values of sample width W is chosen to be the same as in Ref. [4] in order to compare the results with and without the SGF.

For $0.2 < W/l_2$, it is evident that VE resonances appear at $\omega_c \tau_2 = \omega \tau_2 / 2$ for both the two situations $\alpha = 0.9$ and $\alpha = 0$. The width dependence of magnetosonic resonances is determined from Eq. (19). From Fig. 7 one can see that magnetosonic resonances occur for $W/l_2 \leq 3.2$. The number of resonant peaks decreases with W/l_2 . For the narrowest samples $W/l_2 = 0.033$, the magnetosonic resonance dominates and shows a single peak. For all the considered width values, the SGF raises the VE and magnetosonic peaks and almost unchanged the peak positions. The amplification factor depends on the width.

In narrow samples with $W|\lambda| \ll 1$, the velocity $u_x(y)$ as well as the VE flow show a parabolic profile in the whole sample region (not shown here). The linear current response of this high-frequency Poiseuille flow is derived from Eqs. (16) and (2) with the replacement

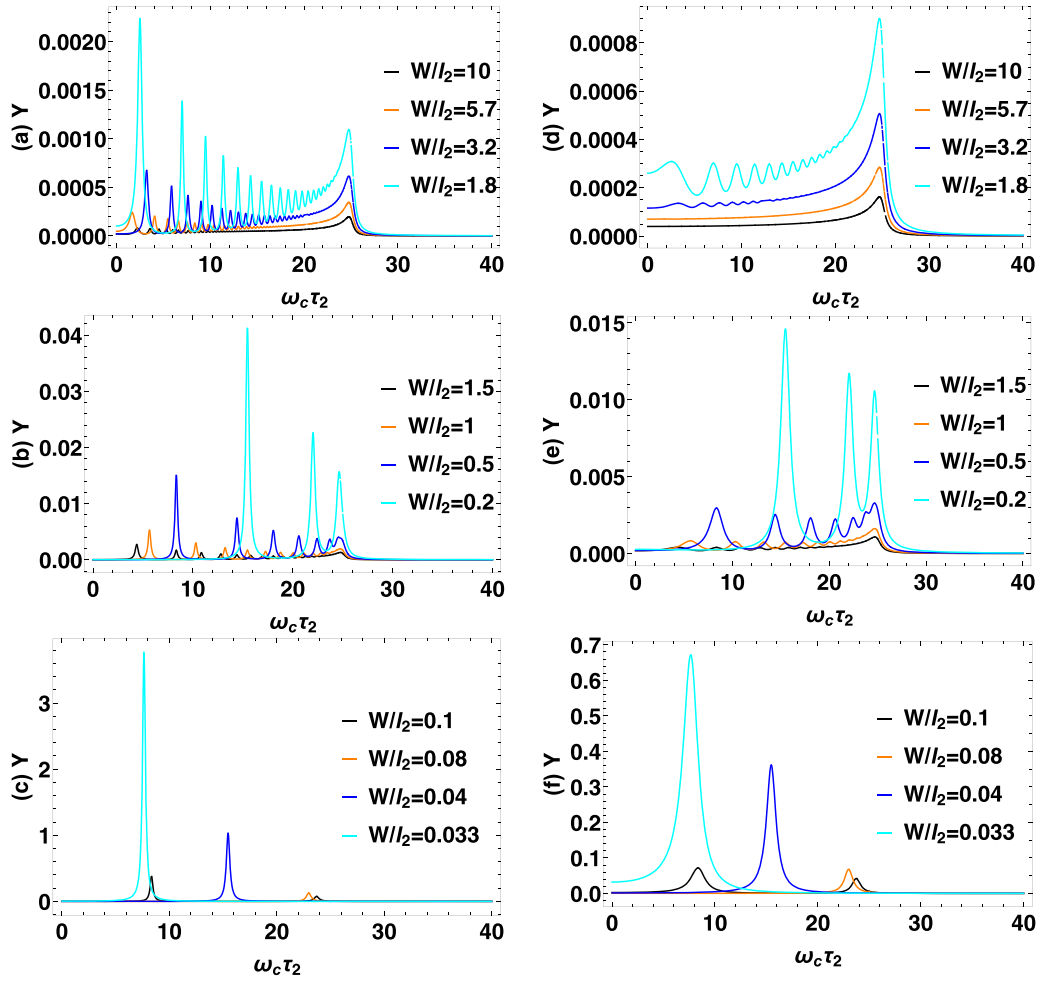


FIG. 7. The absorption power Y in units of Y_0 as a function of $\omega_c \tau_2$ at $\omega \tau_2 = 50$ and $\tau_2/\tau = 10^{-7}$. We take $\alpha = 0.9$ in (a)–(c) and $\alpha = 0$ in (d)–(f). Three regimes of sample width W are considered: (a), (d) medium; (b), (e) narrow; and (c), (f) narrowest.

$\tanh(W\lambda/2) \rightarrow W\lambda/2 - (W\lambda/2)^3/3$. One has

$$I_x = \frac{e^2 n_0 E_0 W^3}{12m} \frac{[(\omega^2 + 4\omega_c^2)\tau_2^2 + i\omega\tau_2^3(-\omega^2 + 4\omega_c^2)]^2}{\eta\omega^2\tau_2^2[(\omega^2 + 4\omega_c^2)\tau_2^2 + i\omega\tau_2^3(-\omega^2 + 4\omega_c^2)] + \omega^4\tau_2^6 F^2 \tau/4}. \quad (25)$$

The SGF dependence of absorption power Y for narrow samples can be obtained directly from this equation. The single Y peak in the AC Poiseuille flow is nearly symmetric due to Eq. (25). In this case, the magnetosonic resonance is directly related to the resonances in the viscosity coefficient $\eta_{xx1}(\omega)$ and manifests itself in the sample absorption power.

Near the VE resonance ($2\omega_c \tau_2, \omega \tau_2 \sim 1$), the AC impedance $Z = E_0/I_x$ obtained from Eq. (25) can be written as

$$Z \approx \frac{12m}{e^2 n_0 W^3} \frac{\eta[1 + i(2\omega_c - \omega)\tau_2] + \tau_2^2 F^2 \tau/4}{[1 + i(2\omega_c - \omega)\tau_2]^2}. \quad (26)$$

In the AC Poiseuille flow, the VE resonance is directly related to the resonances in the viscosity coefficient $\eta_{xx1}(\omega)$ and manifests itself in the sample impedance.

Effect of parameter τ_2/τ . In high-quality GaAs 2DEGs, the relaxation time τ_2 extracted from the magnetoresistance

measurements [6,21,22] approaches 10^{-12} to 10^{-11} s at low temperature ≈ 1 K. For the sample studied in Ref. [9], the ratio τ_2/τ ranges from [2] 0.01 to 0.1. The value $\tau_2/\tau = 10^{-7}$ is assumed for numerical calculations in Ref. [4]. In an InSb 2DEG with high mobility [23], the measured relaxation time τ could reach $\approx 10^{-10}$ s. The ratio $\tau_2/\tau = 10^{-7}$ is difficult to achieve for InSb 2DEG under current experimental progress. It is thus necessary to discuss the effect of τ_2/τ on the robustness of our results. For a fixed $\omega_c \tau_2 = 24.5$, the required magnetic field B_0 for the more realistic value of $\tau_2 = 10^{-11}$ s is about 2 kG, which diminishes as τ_2 increases. Such a magnetic field is easily reachable in experiments.

Figure 8 presents the absorption power Y as a function of $\omega_c \tau_2$ without ($\alpha = 0$) and with ($\alpha = 0.9$) the SGF at three different values of $\tau_2/\tau = 10^{-7}, 10^{-2}, 10^{-1}$. We take $\omega \tau_2 = 50$ and $W/l_2 = 1.8$. In the absence of SGF [Fig. 8(a)], the absorption power Y changes slightly when τ_2/τ increases

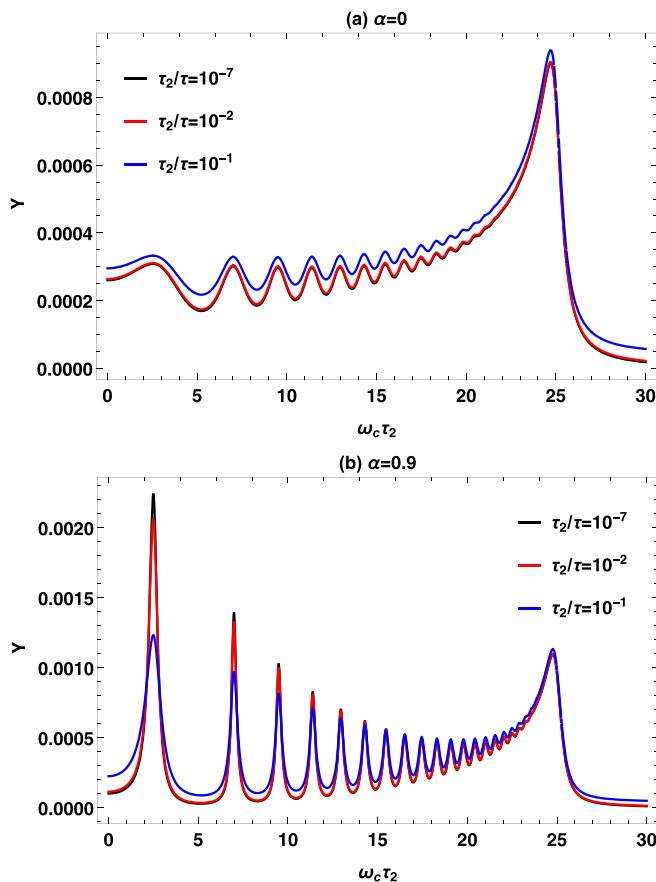


FIG. 8. The absorption power Y in units of Y_0 plotted as a function of $\omega_c \tau_2$ for several values of τ_2/τ . We set $\omega \tau_2 = 50$ and $W/l_2 = 1.8$. (a) $\alpha = 0$; (b) $\alpha = 0.9$.

from 10^{-7} to 10^{-2} . As τ_2/τ varies from 10^{-2} to 10^{-1} , peaks of both VE and magnetosonic resonances move up and do not change their positions. The VE peak is still much higher than the magnetosonic resonant peaks. This can be understood from the two factors in the expression Eq. (16) which determines the absorption power Y . When $\tau_2/\tau \ll \omega \tau_2$, the first factor $\text{Re} \frac{\tau_2}{-i\omega \tau_2 + (\tau_2/\tau)}$ varies almost linearly with τ_2/τ , while the second factor $\text{Im}[1 - \tanh(\lambda W/2)/(\lambda W/2)]$ is almost independent of τ_2/τ .

As shown in Fig. 8(b), the VE resonance changes slightly with τ_2/τ even in the presence of SGF. Here the value F is assumed to decrease with the increase of τ_2/τ so that α is fixed at 0.9. When τ_2/τ increases from 10^{-7} to 10^{-2} , F will reduce by a factor ≈ 316 . In this regime the change of τ_2/τ only has a weak influence on magnetosound resonances (especially for $\omega_c \tau_2 > 10$). Consequently, for the realistic value $\tau_2/\tau = 10^{-2}$, under a much smaller SGF one can achieve remarkable magnetosound resonance with peak much higher than the VE resonance. As τ_2/τ varies from 10^{-2} to 10^{-1} , the first several peaks (satisfying $\omega_c \tau_2 < 10$) of magnetosound resonances decrease obviously. In this case the factor $\text{Im} \tanh(\lambda W/2)$ changes greatly with τ_2/τ for small values of $\omega_c \tau_2$ and large α . It is encouraging to see that even at $\tau_2/\tau = 10^{-1}$ the first magnetosound resonance is still stronger than the VE resonance in the presence of SGF.

IV. CONCLUSIONS AND DISCUSSION

In conclusion, we have used a hydrodynamic method to study the AC transport of viscous electron flow in an InSb 2DEG under an in-plane SGF and a perpendicular magnetic field. In the presence of SGF, the dispersion of the transverse magnetosound waves has two branches and a finite threshold wave vector. Under a linearly polarized external electric field with frequency ω , the absorption power Y varies with the cyclotron frequency ω_c . It exhibits VE resonance at $\omega_c = \omega/2$ and (a series of) transverse magnetosound resonances. For both kinds of resonances, the SGF can raise the peak heights and almost unchanged peak positions. The SGF-induced enhancement of magnetosonic resonances is usually more pronounced than that for the VE resonance and depends on the sample width. The first magnetosonic resonant peak can be tuned by the SGF to be well above the VE peak, which is much lower than the VE peak in the absence of SGF. All of these results arise from the SGF dependence of the effective diagonal viscosity coefficient.

The VE resonance actually has been observed experimentally in photoresistance and photovoltaic effect of GaAs 2DEG systems [24–26] and explained by a hydrodynamic model [4]. However, the transverse magnetosound resonances predicted in Ref. [4] have not been confirmed in experiments. The magnetosound resonances disappear in wide samples and are much weaker than the VE resonance for samples with a medium width. For a medium sample width, we have demonstrated that the SGF can enhance the first magnetosound resonances to be much higher than the VE resonance. This could be helpful for the experimental observation of magnetosound resonances. Our results provide a possible tuning method for the VE resonance and transverse magnetosound resonances, which might be relevant to control the peculiarities in the photoresistance and photovoltaic effects in viscous electron fluids.

ACKNOWLEDGMENTS

This work was supported by the Natural Science Foundation of China through Grants No. 11975174, No. 11774314, No. 11775090, and No. 11775164, and the Fundamental Research Funds for the Central Universities through Grants No. 2020IB023 and No. 2018IB011.

APPENDIX A: FREQUENCY-DEPENDENT VISCOSITY UNDER STERN-GERLACH FORCE

We derive the frequency-dependent viscosity coefficients in the presence of an in-plane Stern-Gerlach force, a perpendicular magnetic field, and an AC electric field with a time dependence $e^{-i\omega t}$.

In the hydrodynamic model, the viscous terms could be described by the viscous stress tensor of a single particle, $\Pi_{i,j} = m \langle v_i v_j \rangle$, where $\mathbf{v} = (v_x, v_y)$ is the two-dimensional velocity of an electron, $i, j \in \{x, y\}$, and the angular bracket is average of the velocity at a fixed point $\mathbf{r} = (x, y)$. Following the approach considered in Refs. [2–4], the momentum balance equation for the hydrodynamic velocity $\mathbf{u} = \langle \mathbf{v} \rangle$ without

Stern-Gerlach force and magnetic field is written as

$$m \frac{\partial u_i}{\partial t} = -\frac{\partial \Pi_{ij}}{\partial x_j} - \frac{m u_i}{\tau} + e E_i. \quad (\text{A1})$$

The viscous stress tensor Π_{ij} can be expressed as [27]

$$\Pi_{ij} = \Pi_{ij}^0 = -m\eta \left(u_{ij} - \frac{1}{2} \delta_{ij} u_{kk} \right), \quad u_{ij} = \frac{\partial u_i}{\partial x_j} + \frac{\partial u_j}{\partial x_i}. \quad (\text{A2})$$

Here $\eta = v_F^2 \tau_2 / 4$ and τ_2 is the second angular momentum relaxation time. This expression of Π_{ij} is derived from the Drude-like equation

$$\frac{\partial \Pi_{ij}}{\partial t} = -\frac{\Pi_{ij} - \Pi_{ij}^0}{\tau_2}. \quad (\text{A3})$$

The magnetic field and Stern-Gerlach force provide additional terms in Eq. (A1) because they can change the hydrodynamic velocity. The expressions for $\frac{\partial \langle v_i \rangle}{\partial t}$ and $\frac{\partial \langle v_i v_j \rangle}{\partial t}$ become

$$\begin{aligned} \left(\frac{\partial \langle v_i \rangle}{\partial t} \right)_{\text{mag}} &= \omega_c \varepsilon_{zik} \langle v_k \rangle, \\ \left(\frac{\partial \langle v_i v_j \rangle}{\partial t} \right)_{\text{mag}} &= \omega_c (\varepsilon_{zik} \langle v_k v_j \rangle + \varepsilon_{zjk} \langle v_j v_k \rangle), \\ \left(\frac{\partial \langle v_i \rangle}{\partial t} \right)_{\text{spin}} &= s F_i, \\ \left(\frac{\partial \langle v_i v_j \rangle}{\partial t} \right)_{\text{spin}} &= s (F_i \langle v_j \rangle + F_j \langle v_i \rangle), \end{aligned} \quad (\text{A4})$$

where $F_i = \frac{g^* \mu_B \partial B_i}{2m \partial x_i} = F$ for $i = y$ while 0 otherwise, $\varepsilon_{zxy} = 1 = -\varepsilon_{zyx}$, and $\varepsilon_{zxx} = \varepsilon_{zyy} = 0$. The terms in Eq. (A4) also appear in Eq. (A3). The latter reads

$$\frac{\partial \Pi_{ij}}{\partial t} = -\frac{\Pi_{ij} - \Pi_{ij}^0}{\tau_2} + s m (F_i \langle v_j \rangle + F_j \langle v_i \rangle) + m \omega_c (\varepsilon_{zik} \langle v_k v_j \rangle + \varepsilon_{zjk} \langle v_i v_k \rangle). \quad (\text{A5})$$

For the viscous flow with an AC frequency of ω , it is convenient to express the time dependence of Π_{ij} as $e^{-i\omega t}$. From Eqs. (A2) and (A5) we obtain

$$(1 - i\omega\tau_2)\Pi_{ij} - \tau_2\omega_c(\varepsilon_{zik}\Pi_{kj} + \varepsilon_{zjk}\Pi_{ik}) - s\tau_2 m(F_i \langle v_j \rangle + F_j \langle v_i \rangle) = -m\eta u_{ij}. \quad (\text{A6})$$

Here we used the relationship $u_{kk} = 0$, which follows from $\nabla \cdot \mathbf{u} = 0$. The components of Π_{ij} fulfill the following relations:

$$\begin{aligned} (1 - i\omega\tau_2)\Pi_{xx} - \tau_2\omega_c(\Pi_{yx} + \Pi_{xy}) &= -m\eta u_{xx}, \\ (1 - i\omega\tau_2)\Pi_{yy} - \tau_2\omega_c(-\Pi_{yx} - \Pi_{xy}) &= -m\eta u_{yy}, \\ (1 - i\omega\tau_2)\Pi_{xy} - \tau_2\omega_c(\Pi_{yy} - \Pi_{xx}) &= -m\eta u_{xy} + A, \\ (1 - i\omega\tau_2)\Pi_{yx} - \tau_2\omega_c(\Pi_{yy} - \Pi_{xx}) &= -m\eta u_{yx} + A, \end{aligned} \quad (\text{A7})$$

where $A = s\tau_2 m F \langle v_x \rangle$. These relations result in

$$\begin{aligned} \Pi_{xx} &= -\frac{1 - i\omega\tau_2}{1 + (-\omega^2 + 4\omega_c^2)\tau_2^2 - 2i\omega\tau_2} m\eta u_{xx} \\ &\quad - \frac{2\omega_c\tau_2}{1 + (-\omega^2 + 4\omega_c^2)\tau_2^2 - 2i\omega\tau_2} m\eta u_{xy} \end{aligned}$$

$$\begin{aligned} &+ \frac{2\omega_c\tau_2}{1 + (-\omega^2 + 4\omega_c^2)\tau_2^2 - 2i\omega\tau_2} A, \\ \Pi_{xy} &= -\frac{1 - i\omega\tau_2}{1 + (-\omega^2 + 4\omega_c^2)\tau_2^2 - 2i\omega\tau_2} m\eta u_{xy} \\ &+ \frac{2\omega_c\tau_2}{1 + (-\omega^2 + 4\omega_c^2)\tau_2^2 - 2i\omega\tau_2} m\eta u_{xx} \\ &+ \frac{1 - i\omega\tau_2}{1 + (-\omega^2 + 4\omega_c^2)\tau_2^2 - 2i\omega\tau_2} A, \end{aligned} \quad (\text{A8})$$

where $\Pi_{xx} = -\Pi_{yy}$ and $\Pi_{xy} = \Pi_{yx}$. We can rewrite Eq. (A8) as

$$\begin{aligned} \Pi_{xx} &= -m\eta_{xx}(\omega)u_{xx} - m\eta_{xy}(\omega)u_{xy} + sm\zeta_y(\omega)\langle v_x \rangle, \\ \Pi_{xy} &= -m\eta_{xx}(\omega)u_{xy} + m\eta_{xy}(\omega)u_{xy} + sm\zeta_x(\omega)\langle v_x \rangle, \end{aligned} \quad (\text{A9})$$

where

$$\begin{aligned} \eta_{xx}(\omega) &= \frac{1 - i\omega\tau_2}{1 + (-\omega^2 + 4\omega_c^2)\tau_2^2 - 2i\omega\tau_2} \eta, \\ \eta_{xy}(\omega) &= \frac{2\omega_c\tau_2}{1 + (-\omega^2 + 4\omega_c^2)\tau_2^2 - 2i\omega\tau_2} \eta, \\ \zeta_x(\omega) &= \frac{1 - i\omega\tau_2}{1 + (-\omega^2 + 4\omega_c^2)\tau_2^2 - 2i\omega\tau_2} \frac{\tau_2 g^* \mu_B}{2m} \frac{\partial B_y}{\partial y}, \\ \zeta_y(\omega) &= \frac{2\omega_c\tau_2}{1 + (-\omega^2 + 4\omega_c^2)\tau_2^2 - 2i\omega\tau_2} \frac{\tau_2 g^* \mu_B}{2m} \frac{\partial B_y}{\partial y}. \end{aligned} \quad (\text{A10})$$

It is convenient to define two effective viscous coefficients as

$$\begin{aligned} \eta_{xx1}(\omega) &= \eta_{xx}(\omega) + \frac{\tau}{4} \zeta_x^2(\omega), \\ \eta_{yx1}(\omega) &= \eta_{yx}(\omega) + \frac{\tau}{4} \zeta_x(\omega)\zeta_y(\omega). \end{aligned} \quad (\text{A11})$$

Note that $\eta_{xx}(\omega)$ and $\eta_{yx}(\omega)$ are the same as in Refs. [3,4].

APPENDIX B: DERIVATION OF EQUATIONS (10) AND (11)

In this Appendix, we give the details for the derivation of Eqs. (10) and (11). At high frequencies ($\omega_c, \omega_q \gg 1/\tau_2 > 1/\tau$) and far from the VE resonance ($|\omega_q - 2\omega_c| \gg 1/\tau_2$), we approximate the factor $[1 + (-\omega^2 + 4\omega_c^2)\tau_2^2 - 2i\omega\tau_2]^{-1}$ in Eq. (2) as $[(4\omega_c^2 - \omega^2)\tau_2^2]^{-1}$ and then separate the real and imaginary part. The results are

$$\text{Re } \eta_{xx1} = \frac{1}{4\omega_c^2 - \omega_q^2} \frac{v_F^2 \eta}{4\tau_2} - \frac{\omega_q^2}{(4\omega_c^2 - \omega_q^2)^2} \frac{F^2 \tau}{4}, \quad (\text{B1})$$

$$\text{Im } \eta_{xx1} = -\frac{\omega_q}{4\omega_c^2 - \omega_q^2} \frac{v_F^2 \eta}{4} - \frac{2\omega_q}{(4\omega_c^2 - \omega_q^2)^2} \frac{F^2 \tau}{4\tau_2}, \quad (\text{B2})$$

$$\text{Im } \eta'_{xx1} = -\frac{v_F^2 \eta}{4} \left[\frac{4\omega_c^2 + \omega_q^2}{(4\omega_c^2 - \omega_q^2)^2} + \frac{2(4\omega_c^2 + 3\omega_q^2)\alpha}{(4\omega_c^2 - \omega_q^2)^3 \tau_2^2} \right]. \quad (\text{B3})$$

Here, the term $O(\omega^{-4})$ is neglected; α and F defined in Eq. (12) are

$$\alpha = \frac{F^2 \tau \tau_2}{v_F^2 \eta}, \quad F = \frac{g^* \mu_B \partial B_y}{2m \partial y}. \quad (\text{B4})$$

By substituting Eq. (B2) into Eq. (8), we obtain

$$\omega_q = -\frac{v_{F\eta}^2 q^2}{4} \omega_q \left[\frac{1}{4\omega_c^2 - \omega_q^2} + \frac{2\alpha}{(4\omega_c^2 - \omega_q^2)^2 \tau_2^2} \right], \quad (\text{B5})$$

which is equivalent to Eq. (10) and can be rewritten as

$$q^2 = \frac{4}{v_{F\eta}^2} \frac{(4\omega_c^2 - \omega_q^2)^2}{[(\omega_q^2 - 4\omega_c^2) - 2\alpha/\tau_2^2]}. \quad (\text{B6})$$

This equation together with the expressions (B1) and (B3) leads to

$$q^2 \text{Re} \eta_{xx1} = \frac{\alpha \omega_q^2 - (4\omega_c^2 - \omega_q^2)}{(4\omega_c^2 - \omega_q^2) \tau_2 + 2\alpha/\tau_2^2}, \quad (\text{B7})$$

$$q^2 \text{Im} \eta'_{xx1} = \frac{16\omega_c^4 - \omega^4 + 2\alpha(4\omega_c^2 + 3\omega_q^2)/\tau_2^2}{[(4\omega_c^2 - \omega_q^2) + 2\alpha/\tau_2^2](4\omega_c^2 - \omega_q^2)}. \quad (\text{B8})$$

By substituting these two equations into the expression of Υ_q in Eq. (9), we get

$$\begin{aligned} \Upsilon_q &= \left[\frac{1}{\tau} + \text{Re}(\eta_{xx1})q^2 \right] / [1 - q^2 \text{Im}(\eta'_{xx1})] \\ &= \frac{\alpha \omega_q^2 - (4\omega_c^2 - \omega_q^2)}{(4\omega_c^2 - \omega_q^2) \tau_2 + 2\alpha/\tau_2} \\ &\quad \times \frac{[(4\omega_c^2 - \omega_q^2) \tau_2 + 2\alpha/\tau_2](4\omega_c^2 - \omega_q^2)}{2\omega_q^2 \tau_2 (\omega_q^2 - 4\omega_c^2 - 4\alpha/\tau_2^2)} \\ &= \frac{(4\omega_c^2 - \omega_q^2)^2 - \alpha \omega_q^2 (4\omega_c^2 - \omega_q^2)}{2\omega_q^2 \tau_2 (4\omega_c^2 - \omega_q^2 + 4\alpha/\tau_2^2)}. \end{aligned} \quad (\text{B9})$$

This is Eq. (11).

APPENDIX C: PROFILES OF HYDRODYNAMIC VELOCITY

In this Appendix, we compare the profile of hydrodynamic velocity under the VE resonance and that for a magnetosound resonance. In Fig. 9 the spatial variation of velocity $u_x(y)$ is plotted for a fixed width $W = 1.8l_2$, frequency $\omega = 50/\tau_2$, and three values of $\omega_c \tau_2 = 25, 7, \text{ and } 2.5$. In the absence of SGF [Fig. 9(a)], it is seen that under VE resonance ($\omega_c \tau_2 = 25 = \omega \tau_2/2$) the velocity $u_x(y)$ decays quickly toward the

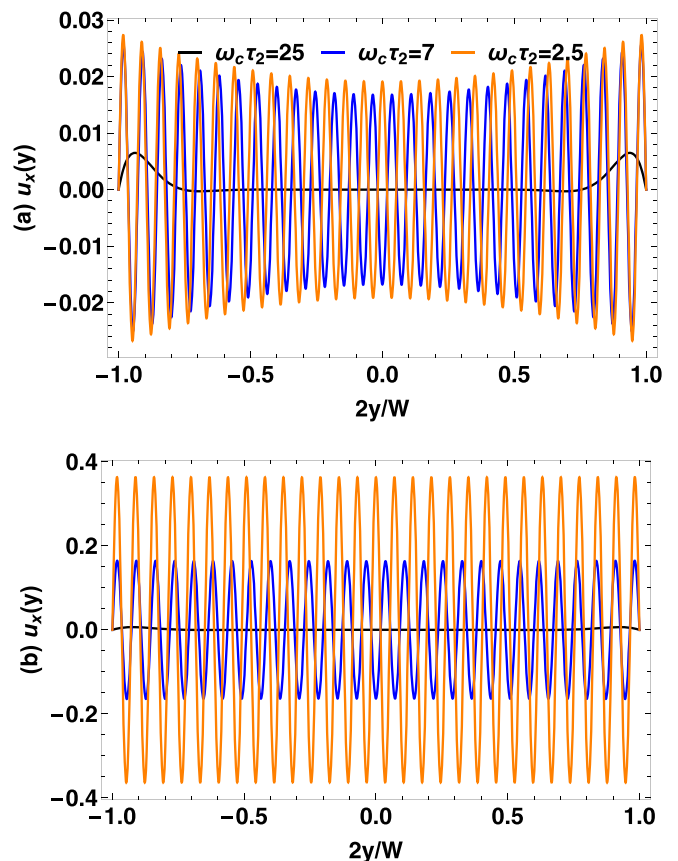


FIG. 9. The distribution of the hydrodynamic velocity $u_x(y)$ in units of $eE_0 \tau_2/m$ as a function of $2y/W$ for several $\omega_c \tau_2$, in the absence ($\alpha = 0$) (a) and presence ($\alpha = 0.95$) (b) of the SGF. Here, $W/l_2 = 1.8$ and $\omega \tau_2 = 50$.

bulk from peaks near either edge of the sample. For magnetosound resonances ($\omega_c \tau_2 \ll \omega \tau_2/2$), the velocity shows obvious oscillations where the amplitude of peaks decays gradually toward the bulk and is much higher than the peak of VE resonance. When a SGF with $\alpha = 0.95$ is applied [Fig. 9(b)], the velocity peaks under magnetosound resonances are enhanced drastically and show only a slight spatial decay. In contrast, the velocity profile under VE resonance shows only a minor change when α varies from 0 to 0.95.

[1] R. N. Gurzhi, *Sov. Phys. Usp.* **11**, 255 (1968).
 [2] P. S. Alekseev, *Phys. Rev. Lett.* **117**, 166601 (2016).
 [3] P. S. Alekseev, *Phys. Rev. B* **98**, 165440 (2018).
 [4] P. S. Alekseev and A. P. Alekseeva, *Phys. Rev. Lett.* **123**, 236801 (2019).
 [5] Y. Zhang, F. Zhai, and W. Jiang, *Phys. Rev. B* **102**, 045133 (2020).
 [6] A. T. Hatke, M. A. Zudov, J. L. Reno, L. N. Pfeiffer, and K. W. West, *Phys. Rev. B* **85**, 081304(R) (2012).
 [7] R. G. Mani, A. Kriisa, and W. Wegscheider, *Sci. Rep.* **3**, 2747 (2013).
 [8] L. Bockhorn, P. Barthold, D. Schuh, W. Wegscheider, and R. J. Haug, *Phys. Rev. B* **83**, 113301 (2011).

[9] Q. Shi, P. D. Martin, Q. A. Ebner, M. A. Zudov, L. N. Pfeiffer, and K. W. West, *Phys. Rev. B* **89**, 201301(R) (2014).
 [10] P. J. W. Moll, P. Kushwaha, N. Nandi, B. Schmidt, and A. P. Mackenzie, *Science* **351**, 1061 (2016).
 [11] M. Semenyakin and G. Falkovich, *Phys. Rev. B* **97**, 085127 (2018).
 [12] R. Moessner, P. Surówka, and P. Witkowski, *Phys. Rev. B* **97**, 161112(R) (2018).
 [13] A. Lucas and S. Das Sarma, *Phys. Rev. B* **97**, 115449 (2018).
 [14] J. Y. Khoo and I. S. Villadiego, *Phys. Rev. B* **99**, 075434 (2019).
 [15] P. S. Alekseev, *Semiconductors* **53**, 1367 (2019).
 [16] A. Imambekov, M. Lukin, and E. Demler, *Phys. Rev. Lett.* **93**, 120405 (2004).

- [17] S. Conti and G. Vignale, *Phys. Rev. B* **60**, 7966 (1999).
- [18] C. Caroli and A. Lemaître, *Phys. Rev. Lett.* **123**, 055501 (2019).
- [19] B. Nedniyom, R. J. Nicholas, M. T. Emeny, L. Buckle, A. M. Gilbertson, P. D. Buckle, and T. Ashley, *Phys. Rev. B* **80**, 125328 (2009).
- [20] Z. Lei, C. A. Lehner, E. Cheah, C. Mittag, M. Karalic, W. Wegscheider, K. Ensslin, and T. Ihn, *Phys. Rev. Res.* **3**, 023042 (2021).
- [21] G. M. Gusev, A. D. Levin, E. V. Levinson, and A. K. Bakarov, *AIP Adv.* **8**, 025318 (2018).
- [22] G. M. Gusev, A. D. Levin, E. V. Levinson, and A. K. Bakarov, *Phys. Rev. B* **98**, 161303(R) (2018).
- [23] C. A. Lehner, T. Tschirky, T. Ihn, W. Dietsche, J. Keller, S. Fält, and W. Wegscheider, *Phys. Rev. Mater.* **2**, 054601 (2018).
- [24] Y. Dai, R. R. Du, L. N. Pfeiffer, and K. W. West, *Phys. Rev. Lett.* **105**, 246802 (2010).
- [25] A. T. Hatke, M. A. Zudov, L. N. Pfeiffer, and K. W. West, *Phys. Rev. B* **83**, 121301(R) (2011).
- [26] M. Białek, J. Lusakowski, M. Czapkiewicz, J. Wróbel, and V. Umansky, *Phys. Rev. B* **91**, 045437 (2015).
- [27] L. D. Landau and E. M. Lifshitz, *Fluid Mechanics* (Pergamon Press, Oxford, 1987).